Materials Today Bio 24 (2024) 100925

Contents lists available at ScienceDirect

Materials Today Bio

journal homepage: www.journals.elsevier.com/materials-today-bio

Live macrophages loaded with Fe_3O_4 and sulfasalazine for ferroptosis and photothermal therapy of rheumatoid arthritis

Li Ruan [a,b,1], Xinxi Cai [a,b,1], Rui Qian [a,b,1], Shifang Bei [c], Lin Wu [a,**], Jin Cao [b], Song Shen [b,*]

[a] Affiliated Hospital of Jiangsu University, Zhenjiang, 212001, China
[b] College of Pharmaceutical Sciences, Jiangsu University, Zhenjiang, Jiangsu, 212013, China
[c] The Affiliated People's Hospital, Jiangsu University, Zhenjiang, Jiangsu, 212001, China

ARTICLE INFO

Keywords:
Rheumatoid arthritis
Iron oxide nanoparticles
Macrophages
Ferroptosis
Drug delivery
Photothermal therapy

ABSTRACT

Rheumatoid arthritis (RA) is a systemic autoimmune disease characterized by the infiltration of inflammatory cells and proliferation of synovial cells. It can cause cartilage and bone damage as well as disability and is regarded as an incurable chronic disease. Available therapies cannot prevent the development of diseases due to the high toxicity of the therapeutic agents and the inefficient drug delivery. Ferroptosis, an iron-dependent manner of lipid peroxidative cell death, indicates great potential for RA therapy due to ability to damage the infiltrated inflammatory cells and proliferated fibroblast-like synoviocytes. Here, we use macrophages as vector to deliver Fe_3O_4 nanoparticles and sulfasalazine (SSZ) for ferroptosis and photothermal therapy of RA. The inherent property of migration towards the inflamed joints under the guidance of inflammatory factors enables macrophages to targetedly deliver the payload into the RA. Upon the irradiation of the near infrared light, the Fe_3O_4 nanoparticles convert the light into heat to damage the proliferated synovium. Meanwhile, the iron released from Fe_3O_4 nanoparticles works with SSZ to generate synergetic ferroptosis effect. The resident inflammatory cells and proliferated synovium are efficiently damaged by the ferroptosis and photothermal effect, showing pronounced therapeutic effect for RA.

1. Introduction

Rheumatoid arthritis (RA) is an autoimmune disease characterized by the infiltration of immune cells and the proliferation of fibroblast-like synoviocytes (FLSs). The proliferated FLSs will damage the cartilage and bone, leading to the disability [1–3]. Generally, RA is regarded as an incurable chronic disease, since the aetiology is unknown and no causal treatment is available [4,5]. Recently, non-steroidal anti-inflammatory drugs (NSAIDs), corticosteroids and disease-modifying anti-rheumatic drugs (DMARDs) aiming to block the inflammatory cytokines and inhibit the immune response are widely used for the treatment of RA [6,7]. However, these drugs will cause various adverse effects including high cytotoxicity, immunosuppression, infections, and interstitial lung disease [8,9]. Meanwhile, the hyperplastic FLSs, which mediates the destruction of cartilage and bone, cannot be eliminated efficiently by existing methods [10]. Therefore, alternative treatment strategies which can precisely deliver the drug into the inflamed sites and damage the proliferated FLSs are urgently needed for efficient RA therapy.

Ferroptosis is a novel form of regulated cell death mediated by iron-dependent lipid peroxidation and membrane damage [11–13]. In the inflammatory microenvironments such as tumor and RA [14], the hydrogen peroxide (H_2O_2) is enriched and can be catalyzed by Fe^{2+}-mediated Fenton reaction to generate highly toxic •OH. The •OH induces the intracellular lipid peroxidation (LPO) and causes damage to the hyperplastic FLSs and infiltrated immune cells, showing a great potential for RA therapy. However, the cells have perfect antioxidant system to eliminate excess iron and remove the peroxides by upregulating the ferroportin and glutathione peroxidase 4 (GPX4) [15,16]. Ferroptosis inducers, such as sulfasalazine (SSZ) and erastin, can inhibit the cell membrane cystine/glutamate transporter (known as system xc^-) to decrease the import of cysteine and subsequently downregulate the antioxidant glutathione (GSH) and GPX4 [17–20]. Hence, the SSZ is expected to generate synergistic ferroptosis effect with iron. Fe_3O_4 nanoparticles (NPs) have been widely applied as contrast agent for

* Corresponding author.
** Corresponding author.
E-mail addresses: linmeimei1983@163.com (L. Wu), jsdx.shensong@163.com (S. Shen).
[1] Contributed equally.

https://doi.org/10.1016/j.mtbio.2023.100925
Received 17 September 2023; Received in revised form 26 November 2023; Accepted 18 December 2023
Available online 20 December 2023

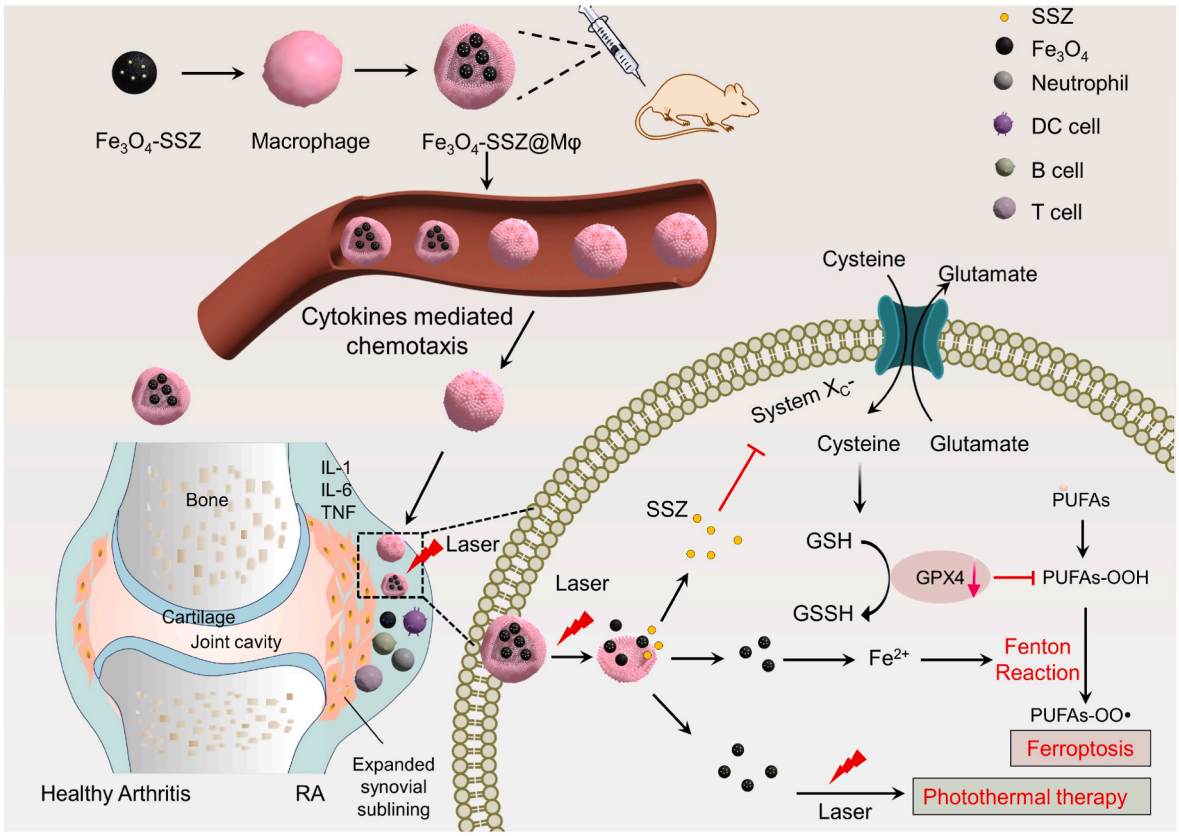

Scheme 1. Schematic illustration of Mφ-mediated drug delivery for ferroptosis and photothermal therapy of RA. SSZ is firstly loaded onto the Fe_3O_4 NPs (Fe_3O_4-SSZ). Then, the Fe_3O_4-SSZ NPs are endocytosed by Mφ to fabricate Fe_3O_4-SSZ@Mφ. After intravenous injection, cytokines guide the migration of Fe_3O_4-SSZ@Mφ along the chemotactic gradient. Fe_3O_4-SSZ@Mφ penetrates into the RA tissue and releases the Fe_3O_4 and SSZ upon the activation of NIR light. SSZ inhibits the system xc^- to downregulate the GSH and GPX4 and works with Fe_3O_4 to induce ferroptosis effect. Meanwhile, the PTT enhances the ferroptosis effect to generate synergistic killing effect towards hyperplastic FLSs and infiltrated immune cells.

magnetic resonance imaging in clinic and can be dissolved in acidic environment to release Fe^{2+} for the ferroptosis therapy. Meanwhile, Fe_3O_4 NPs exhibit excellent photothermal effect [21,22] and can be served as photothermal agent to ablate hyperplastic FLSs. Although nanoparticles can be accumulated in RA due to the enhanced permeability and retention effect (just like the tumor), the targeting efficiency of the Fe_3O_4 NPs for RA is low and needs to be further improved.

As immune cells, macrophages (Mφ) involving in innate and adaptive immunity can recruit to the inflammation site under the guidance of the chemokines and cytokines, providing a clue for the active targeting drug delivery for RA. Meanwhile, the macrophages can protect the nanoparticles from being quick cleared from the body and prolong the blood circulation time. Here, we developed engineering macrophages loaded with Fe_3O_4 and SSZ for ferroptosis and photothermal therapy of RA (Scheme 1). By employing the inherent inflammation chemotaxis of Mφ, Fe_3O_4 NPs and SSZ can be effectively transported into the RA tissue. While irradiated with near infrared (NIR) light, Fe_3O_4 NPs generate heat and destroy the Mφ to release Fe_3O_4 NPs and SSZ, leading to ferroptosis of the proliferated FLSs and infiltrated immune cells. Meanwhile, it is reported that photothermal therapy (PTT) can work with ferroptosis to enhance the therapeutic effect [23–27]. Hence, this hybrid platform is believed to realize better killing effect towards FLSs and immune cells, so as to inhibit the arthritis.

2. Experimental

2.1. Materials

Ferric chloride hexahydrate ($FeCl_3 \bullet 6H_2O$), trisodium citrate dehydrate (Na_3Cit), sodium acetate trihydrate ($NaAc \bullet 3H_2O$), ethylene glycol (EG), polyethylene glycol (PEG, Mw = 4000), anhydrous ethanol and dimethyl sulfoxide (DMSO) were acquired from Sinopharm Chemical Reagent Co., Ltd. (China). Sulfasalazine (SSZ) and doxorubicin hydrochloride (DOX) were generously granted by Energy Chemical. Thiazolyl blue tetrazolium bromide (MTT), coumarin-3-carboxylic acid (3-CCA) and Hoechst 33,342 were purchased from Sigma-Aldrich. All needing reagents were utilized without further disposal. Deionized water was manufactured by Milli-Q system (Millipore, USA) and employed throughout the experiments.

2.2. Cell culture

Murine RAW264.7 cells were cultured in DMEM medium (Gibco, USA) supplemented with 10 % fetal bovine serum (FBS) and 1 % (v/v) penicillin/streptomycin at 37 °C in humidified atmosphere with 5 % CO_2.

2.3. Synthesis of iron oxide nanoparticles (Fe_3O_4 NPs)

Ethylene glycol (47 mL) was used as solvent to dissolve the PEG 4000 (0.333 g), $FeCl_3 \bullet 6H_2O$ (0.530 g) and trisodium citrate (0.466 g) followed by vigorous stirring to form a clear mixture at room temperature (RT). With the adding of NaOAc (2.790 g), the mixture was further vigorously stirred for 1 h and then transferred to into a Teflon-lined stainless-steel autoclave. Hydrothermal reactions were conducted at 200 °C for 10 h. Black product was collected by centrifugation (13,000 rpm, 30 min) and washed with ethanol for three times.

2.4. Synthesis and characterization of Fe_3O_4-SSZ NPs

SSZ was loaded into the Fe_3O_4 NPs by physical absorption due to the small size and large surface area. To fabricate Fe_3O_4-SSZ, 0.1 mL of SSZ solution (30 mg/mL, in DMSO) was mixed with 5 mL Fe_3O_4 suspension (10 mg, in water) overnight. Then, Fe_3O_4-SSZ NPs were collected by centrifugation (13,000 rpm, 20 min) and washed with DMSO/H_2O (v/v, 1/49) solution to remove the unbound SSZ. To determine the encapsulation efficacy (EE) and loading capacity (LC), the SSZ in the supernatant was determined by UV–vis spectroscopy at the wavelength of 359 nm. Then the EE and LC was calculated by $LC = W_{\text{loaded drug}}/W_{\text{total}} \times 100\ \%$ and $EE = W_{\text{loaded drug}}/W_{\text{feeded drug}} \times 100\ \%$, respectively. Where, the $W_{\text{loaded drug}}$ is the weight of loaded drug, W_{total} is weight of the Fe_3O_4-SSZ, $W_{\text{feeded drug}}$ is weight of the feeded drug.

The morphology of the Fe_3O_4 and Fe_3O_4-SSZ NPs was characterized by transmission electron microscopy and (TEM, JEM-2100, JEOL, Japan) and the scanning electron microscope (SEM, Quanta 200, Netherlands). The size distribution and zeta potentials of the Fe_3O_4 and Fe_3O_4-SSZ NPs were analyzed using dynamic light scattering (DLS, NanoBrook 90Plus, Brookhaven, USA). The FTIR and UV–vis spectra of Fe_3O_4 and Fe_3O_4-SSZ NPs were recorded on Fourier transform infrared spectroscope (FTIR-370, Nicolet Avatar, US) and UV–vis spectrophotometer (Lambda 900, PerkinElmer, US), respectively. The blood compatibility was performed by incubating the Fe_3O_4-SSZ NPs (with Fe_3O_4 concentration of 0, 50, 100, 200, 400, 600, 800 and 1000 μg/mL) with 2 % red cell suspension.

2.5. In vitro •OH generation

The production of •OH was determined using coumarin-3-carboxylic acid (3-CCA) as probe, which is non-fluorescent and can react with •OH to generate fluorescent 3-carboxy-7-hydroxycoumarin (7-OH-3-CCA). 1 mL of Fe_3O_4-SSZ (with Fe_3O_4 concentration of 2 mg/mL) were dispersed in 1 mL of PBS with pH of 4.0, 5.5, and 7.4 for different times (0, 2, 4, 6 and 8 h). For irradiation groups, the solution was exposed to NIR laser (808 nm) for 5 min at a power intensity of 2 W/cm^2. At certain time intervals, the supernatant of the Fe_3O_4-SSZ NPs was collected by centrifugation (13,000 rpm, 10 min) and incubated with H_2O_2 (1 M, 100 μL) and 3-CCA (1 mM, 200 μL) for 30 min. Subsequently, the fluorescence of solution was measured by spectrophotometer.

2.6. Photothermal effect of Fe_3O_4-SSZ

In vitro photothermal properties of the Fe_3O_4-SSZ were studied by exposing the suspensions (with Fe_3O_4 concentration of 20, 50, 100, 200 and 500 μg/mL) to 808 nm laser at a power intensity of 2 W/cm^2 for 5 min. The temperature of the suspension during irradiation was measured using a thermocouple thermometer (Victor, China), Meanwhile, the suspensions were imaged by Thermal Camera (Testo 875-1, Germany). For the photothermal stability study, Fe_3O_4-SSZ NPs were repeatedly irradiated with NIR laser for 5 cycles with each cycle lasting for 5 min.

2.7. In vitro SSZ release from Fe_3O_4-SSZ NPs

In vitro SSZ release was performed by dispersing Fe_3O_4-SSZ NPs in 5 mL of PBS with pH of 5.3 and 7.4 (with SSZ concentration of 2 mg/mL). The dispersion was stirred at 37 °C in the presence and absence of NIR irradiation (808 nm, 2 W/cm^2) for 5 min. At predetermined time points (2, 4, 6, 8, 12 and 24 h), the supernatant was collected by centrifugation (12,000 g, 1 h, 4 °C) and measured at 359 nm by UV–Vis spectrophotometer. After the determination, fresh PBS (5 mL) was supplemented for continued incubation. Fe_3O_4-SSZ NPs dispersed in pH 5.3 for 24 h were collected by centrifugation for TEM imaging.

2.8. Preparation of Fe_3O_4-SSZ@Mφ

To fabrication of Fe_3O_4-SSZ@Mφ, Fe_3O_4-SSZ NPs were incubated with macrophages at different concentrations (with SSZ concentration of 10, 20, 40 and 80 μg/mL) for 0.5, 1, 2 and 4 h. Then, the cells were collected and dispersed in aqua regia to determine intracellular Fe contents by inductively coupled plasma emission spectrometer (ICP-OES). Meanwhile, cells were collected and digested to determine the intracellular loaded SSZ. The cells were disrupted by ultrasound and followed by dispersing in DMSO. Then the supernatant was collected to determine the SSZ content by UV–vis spectrophotometer. Furthermore, 2.0 mL Fe_3O_4 suspension (5 mg/mL) was added to 1.0 mL FITC solution (2 mg/mL) under ultrasound, and then the mixtures were oscillated for 12 h at RT. After centrifugation at 14,000 rpm for 30 min, the produced Fe_3O_4-FITC NPs were collected and dispersed in PBS. Then FITC-labeled Fe_3O_4 NPs (with FITC concertation of 10, 20, 40 and 80 μg/mL) were incubated with macrophages for 4 h. Then, the cell was gathered by cell scraper, pelleted by centrifugation (1500 rpm, 5 min) and dispersed in the PBS with ice bath for flow cytometry examination. What's more, Fe_3O_4 NPs loaded macrophages were characterized by TEM to observe the distribution of the NPs in the cells.

2.9. Uptake of Fe_3O_4 NPs in Mφ

To study the cellular uptake, DOX, a nucleophilic dye, was used as probe to label the Fe_3O_4 NPs (The preparation process was the same with Fe_3O_4-FITC NPs). Macrophages were seeded onto the dishes for 24 h and then incubated with free DOX and DOX-labeled Fe_3O_4 NPs with DOX concentration of 10 μg/mL for 1 h and 4 h. With or without laser irradiation for 5 min (808 nm, 2 W/cm^2), the cells were stained with Hoechst 33,342 (10 μg/mL) for 15 min and observed by confocal laser scanning microscope (CLSM, TSM800, Leica, Germany).

Quantitative cellular uptake was performed by flow cytometry (ORFLO, USA). After incubation with free DOX and DOX-labeled Fe_3O_4 NPs at DOX concentration of 10 μg/mL, the macrophages were irradiated with 808 nm laser at a power intensity of 2 W/cm^2 for 5 min. Subsequently, the cells were collected for flow cytometry examination. Cells without NIR laser irradiation were used as control.

2.10. Isolation and culture of FLSs

To isolate the FLSs, CIA mice were sacrificed and the synovial tissue was collected aseptically. The synovial tissue was cut into tissue blocks with 2 mm^3 and incubated with culture medium to facilitate synoviocytes migration and growth. Then, the cells were cultured and the tissues were discarded. The morphology of FLSs (1st to 4th generations) was observed by microscope. Immunocytochemical staining was performed to characterize the vimentin of FLSs, which is considered as a feature of FLSs. The chemoimmunology experiment was carried out according to the manufacturer's specification.

2.11. Macrophages migration and polarization assay

Migration ability is critical for Mφ to deliver the drugs into RA tissue and may be affected by the Fe_3O_4-SSZ NPs. The influence of Fe_3O_4-SSZ on the migration of Mφ was evaluated by a transwell experiment. In the experiment, Fe_3O_4-SSZ@Mφ or untreated macrophages suspended in FBS-free DMEM medium were seeded into the upper chamber of separate inserts. FLSs in 500 μL of DMEM containing 10 % FBS were added to the 24-well plates. After incubation for 24 h, the migrated cells were fixed with 4 % paraformaldehyde and stained with 0.1 % crystal violet for 20 min. After washing with PBS, the cells were imaged with microscope.

Macrophages have two phenotypes: M1 and M2 macrophages, which are characterized by the secretion of pro-inflammatory cytokines tumor necrosis factor-α (TNF-α), interleukin-6 (IL-6), IL-1β, and anti-

inflammatory cytokines IL-10, respectively. The loading of Fe_3O_4-SSZ NPs may affect the phenotype of macrophages. After incubation with Fe_3O_4-SSZ NPs (40 μg/mL), the phenotype of macrophages was studied by measuring the secreted cytokines including IL-1β, IL-6, TNF-α, and IL-10 by enzyme-linked immunosorbent assay (ELISA). Meanwhile, M1 type macrophages were induced as control by incubation with lipopolysaccharide (LPS, 1 μg/mL) for 24 h. The morphology of the macrophages after different treatments was imaged by the microscope.

2.12. Cytotoxicity of Fe_3O_4-SSZ to macrophages

The cytotoxicity of SSZ, Fe_3O_4, and Fe_3O_4-SSZ to macrophages was studied. Macrophages were incubated with SSZ (0, 1.5, 7, 15, 30, and 70 μg/mL), Fe_3O_4 and Fe_3O_4-SSZ (with Fe_3O_4 concentration of 0, 10, 50, 100, 200, and 500 μg/mL) for 24 h. The irradiation groups were exposed to 808 nm laser at a power intensity of 2 W/cm^2 for 5 min after incubation for 4 h. Then, the cells were incubated for another 20 h and the cell viability was measured by MTT.

The live/dead cell staining was also utilized to verify the cell viability. Macrophages were seeded in 6-well plate for 24 h and then incubated with SSZ (30 μg/mL), Fe_3O_4 or Fe_3O_4-SSZ (with Fe_3O_4 concentration of 200 μg/mL). 4 h later, the irradiation groups were exposed to 808 nm laser at a power intensity of 2 W/cm^2 for 10 min. Then, the cells were stained with live/dead cell kit with calcein-AM for live cells and propidium iodide (PI) for dead cells. Followed by fixing with 4 % paraformaldehyde for 30 min, the cells were observed by CLSM.

The toxicity of Fe_3O_4-SSZ might be due to the ferroptosis induced by Fe_3O_4 and SSZ. To explore the toxic mechanism, anti-ferroptosis agents were used to study their effect on the cell viability. Macrophages were seeded in 96-well plate for 24 h and then incubated with vitamin E (VE, 1, 10 and 20 μM), GSH (0.5, 1 and 2 mM), or deferoxamine mesylate (DFOM, 100, 200 and 500 μM) for 6 h. Then, the cells were incubated with Fe_3O_4-SSZ at Fe_3O_4 concentration of 500 μg/mL for another 24 h. The cell viability was determined by MTT assay.

The toxic mechanism of the Fe_3O_4-SSZ was further studied by determining the intracellular levels of GSH, GPX4, and malondialdehyde (MDA). After incubation with SSZ (10, 40 and 100 μg/mL), Fe_3O_4 and Fe_3O_4-SSZ (at Fe_3O_4 concentration of 70, 280 and 700 μg/mL) for 24 h, the GSH, GPX4, and MDA were measured by GSH, GPX4, and MDA assay kit according to the manufacturer's instruction.

2.13. Cellular free radical and LPO assay

SSZ and Fe_3O_4 induced ferroptosis by producing free radicals, which led to LPO. The generated ROS and •OH were measured by using 2′, 7′-dichlorofluorescein diacetate (DCFH-DA) and coumarin-3-carboxylic acid (3-CCA) as probes, respectively. Macrophages were seeded onto 96-well plate for 24 h and incubated with SSZ (70 μg/mL), Fe_3O_4 and Fe_3O_4-SSZ NPs (at Fe_3O_4 concentration of 500 μg/mL) for another 24 h. Then, the culture media were removed. The cells were washed and stained with DCFH-DH (10 μM) and Hoechst 33,342 (10 μg/mL) for 30 min and 15 min to detect the total ROS. To measure the •OH, cells were stained with 3-CCA (10 μM) and LysoGreen (1 μM) for 45 min and 30 min, respectively. The lipid peroxidation was also monitored by using C11BODIPY$^{581/591}$ as probe. After the treatment of SSZ, Fe_3O_4 and Fe_3O_4-SSZ NPs, cells were incubated with C11-BODIPY$^{581/591}$ fluorescent probe (10 μM) for 30 min. After the treatment, cells were imaged by CLSM.

2.14. Cytotoxicity of Fe_3O_4-SSZ@Mφ against FLSs

To study the cytotoxicity of Fe_3O_4-SSZ@Mφ to FLSs, Fe_3O_4-SSZ@Mφ (1×10^6 cells, 2 mL culture medium for each group) were added into six-well plate. 2 mL of the released drugs (including free SSZ and Fe_3O_4-SSZ) at predetermined time points (6, 12, 24, and 48 h) was collected under the irradiation of NIR laser (808 nm, 2 W/cm^2, 10 min). Then collected samples were incubated with adherent FLSs (at density of 1×10^5 cells per well). After incubation for 4 h, the cells were irradiated with 808 nm laser for 10 min (the photothermal temperature is controlled below 43 °C by adjusting the intensity of the laser). The cell viability was measured by MTT for another 20 h.

2.15. Biodistribution study

Collagen induced arthritis (CIA) model mice were established by immunization with type II collagen in complete Freund's adjuvant (CFA). Bovine type II collagen dissolved in the acetic acid (0.1 M) was mixed with complete freund's adjuvant to prepare the solution with collagen concentration of 1 mg/mL. The mixture was emulsified in ice bath to obtain the adjuvant. Then, the adjuvant was subcutaneously injected into the planta pedis of the right hind paw at a dosage of 50 μL per mice for twice (at the first and fourteenth day). During the immunization, the thicknesses of paws were measured by a vernier caliper. It taken about 28 d to establish the CIA model. All animal experiments were performed in accordance with the Guidelines for Care and Use of Laboratory Animals of Jiangsu University and approved by the Animal Ethics Committee of Jiangsu University.

To study the targeting effect of the macrophages, the biodistribution of the Fe_3O_4 and Fe_3O_4@Mφ was investigated. Indocyanine green (ICG), a near infrared fluorescent dye, was used as probe to label the nanoparticles (The preparation process was the same with Fe_3O_4-FITC NPs). Free ICG, Fe_3O_4-ICG and Fe_3O_4-ICG@Mφ were intravenously injected into the CIA mice at ICG dosage of 2 mg/kg. At the scheduled times (2, 6, 12, 24 and 48 h), the mice were sacrificed and the major tissues and joint tissues were harvested for fluorescence imaging.

2.16. In vivo photothermal effect

CIA mice were divided into three groups to receive saline, Fe_3O_4 NPs and Fe_3O_4@Mφ at Fe_3O_4 dosage of 2 mg/kg 24 h later, the inflamed paws were irradiated with 808 nm laser at a power density of 2 W/cm^2 for 5 min. The temperatures of the paws were recorded by thermocouple thermometer. Meanwhile, the paws were imaged by thermal infrared camera to vividly monitor the temperature.

2.17. In vivo therapeutic effects study

CIA mice were randomly divided into eight groups (n = 5): a) saline, b) laser, c) Fe_3O_4, d) SSZ, e) Fe_3O_4-SSZ, f) Fe_3O_4-SSZ@Mφ, g) Fe_3O_4-SSZ@Mφ + laser, h) Fe_3O_4-SSZ@Mφ + laser. The SSZ, Fe_3O_4-SSZ and Fe_3O_4-SSZ@Mφs were intravenously injected at SSZ dosage of 5 mg/kg. The dosage of Fe_3O_4 group was 35 mg/kg. For the laser groups, the RA paws were irradiated with 808 nm laser at a power density of 2 W/cm^2 for 5 min after intravenous injection for 12 h. The treatment was carried out every 4 d for total 5 times. During the therapy, body weight and thickness of paws during the treatment were recorded. Paw inflammation was scored visually as follows: 0 = normal paw; 1 = one toe inflamed and swollen; 2 = more than one toe but not the entire paw inflamed and swollen, or mild swelling of entire paw; 3 = erythema and moderate swelling extending to the entire paw; and 4 = severe erythema and swelling of the whole paw and ankle. Each paw was graded with a score from 0 to 4, generating an arthritis score on a scale of 0–4 for each individual mouse. At the end the experiment, the mice were sacrificed and serum was collected for the analysis of pro-inflammatory cytokines. The cytokines including TNF-α and IL-1β were determined by ELISA kit. In addition, the main tissues and inflamed joints were obtained to perform the hematoxylin-eosin (HE) staining. And the inflamed joints were collected for safranin O/fast green staining and immunohistochemical staining of GPX-4.

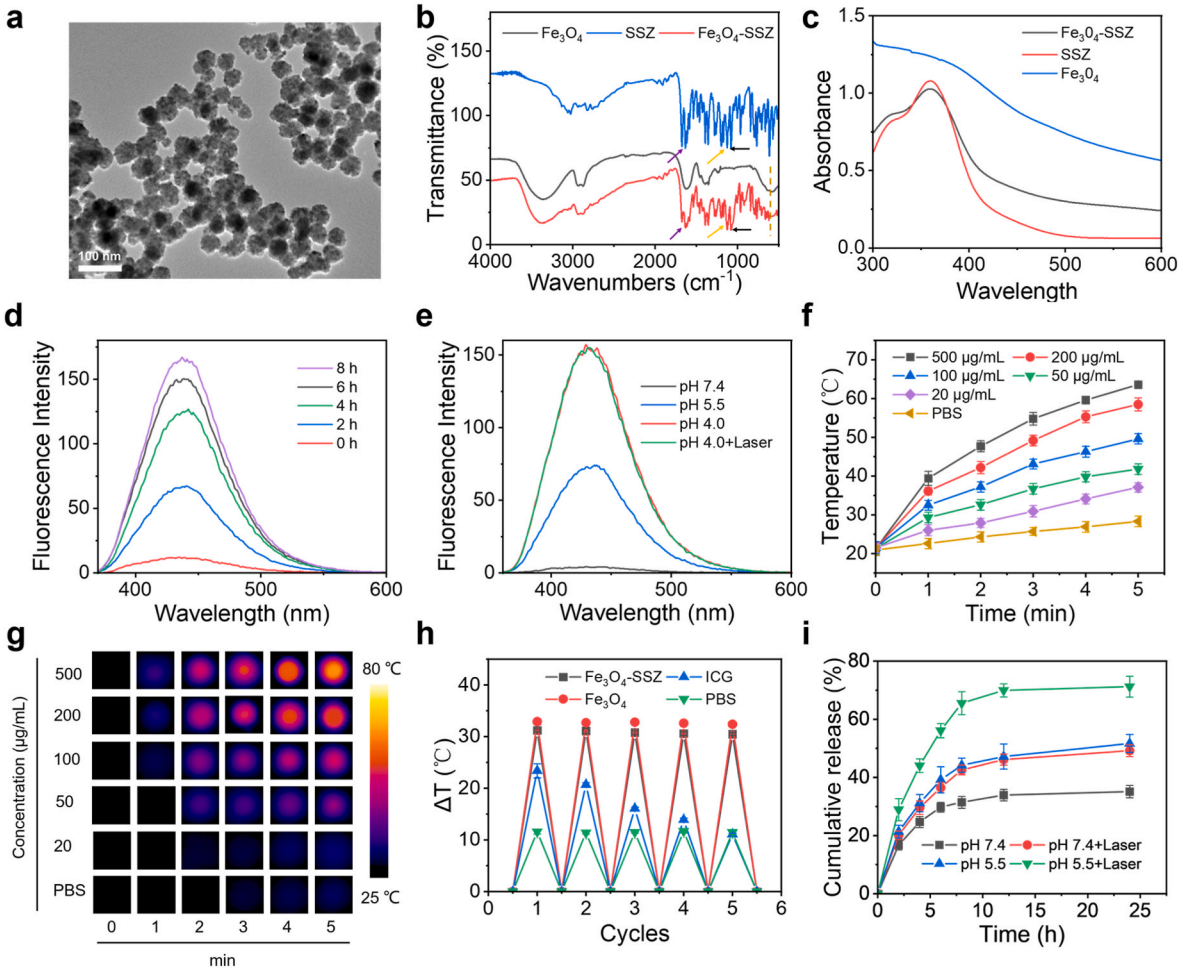

Fig. 1. (a) TEM images of Fe_3O_4-SSZ NPs. (b) The FTIR spectra of SSZ, Fe_3O_4 and Fe_3O_4-SSZ NPs. Purple, yellow, and black arrows indicated C═O (1641 cm^{-1}), C═N (1173 cm^{-1}), and C–O peak (1082 cm^{-1}), respectively. Yellow dotted line indicated Fe–O peak (581 cm^{-1}). (c) The UV–Vis spectra of SSZ, Fe_3O_4 and Fe_3O_4-SSZ NPs. The fluorescence of •OH generated by Fe_3O_4-SSZ mediated Fenton reaction in various time intervals (0, 2, 4, 6 and 8 h) (d) or different pH (4.0, 5.5 and 7.4) (e) with or without NIR laser irradiation. (f) Temperatures of PBS and Fe_3O_4-SSZ NPs with various concentrations after irradiation with 808 nm laser at an intensity of 2 W/cm^2 for 5 min. (g) Infrared thermographic images of Fe_3O_4-SSZ NPs with various concentrations after the irradiation of NIR laser. (h) Photothermal stability of PBS, ICG, Fe_3O_4 and Fe_3O_4-SSZ NPs upon the NIR irradiation for repeated 5 cycles. (i) Release profiles of SSZ from Fe_3O_4-SSZ NPs in pH 5.5 and 7.4 in the presence and absence of NIR irradiation.

3. Results and discussion

3.1. Characterization of Fe_3O_4-SSZ NPs

Fe_3O_4 NPs were prepared by solvothermal method and characterized by TEM and SEM. As shown in Figs. S1a and b, the Fe_3O_4 NPs were monodispersed, showing a spherical shape and average size of ~40 nm. Loading of SSZ showed negligible effect on the disperse of the NPs (Fig. 1a). The average hydrodynamic diameters of Fe_3O_4 and Fe_3O_4-SSZ NPs were determined by DLS to be 55 nm and 68 nm, respectively (Fig. S2). After loading of SSZ, the zeta potentials of Fe_3O_4 slightly increased from −17.58 mV to −11.82 mV (Fig. S3). FTIR spectrum of Fe_3O_4-SSZ NPs showed the characteristic peaks of Fe_3O_4 NPs (Fe–O peak of 581 cm^{-1}) and SSZ (C–O peak of 1082 cm^{-1} and C═N peak of 1173 cm^{-1}), indicating the successful loading of SSZ (Fig. 1b). The successful preparation of Fe_3O_4-SSZ was further verified by the UV–Vis spectra that characteristic absorption peak of SSZ at 359 nm was found in the spectrum of Fe_3O_4-SSZ NPs (Fig. 1c). The encapsulation efficacy and loading capacity of SSZ on Fe_3O_4 NPs was determined to be 49.19 % and 12.86 %, respectively. Fe_3O_4-SSZ NPs showed good blood compatibility that no obvious hemolysis was found after incubation red blood cells at different concentrations (Fig. S4).

3.2. In vitro •OH production

The Fe_3O_4-SSZ NPs can dissolve in the acidic environment and release iron ion to catalyze the Fenton reaction and produce •OH. We incubated the Fe_3O_4-SSZ NPs with H_2O_2 and monitored the generation of •OH by using coumarin-3-carboxylic acid (3-CCA) as an indicator, which can react with •OH to generate fluorescent 7-Hydroxycoumarin-3-carboxylic Acid (7-OH-3-CCA). As shown in Fig. 1d, the fluorescent intensity increased as the incubation time extended. Meanwhile, the pH of the solution showed remarkable influence on the generation of •OH that bright fluorescence was observed in the pH 4.0 solution (Fig. 1e). By contrast, only extremely weak fluorescence was detected in the pH 7.0 solution. These results indicate the pH sensitive release of Fe^{2+} and also the pH sensitive Fenton reaction.

3.3. Photothermal effect of Fe_3O_4-SSZ NPs

The photothermal effect of Fe_3O_4-SSZ NPs was studied by irradiation with NIR light (808 nm) at a power density of 2 W/cm^2. As shown in Fig. 1f, the temperature increased as the concentrations of NPs and irradiation time increased. After irradiation for 5 min, the temperatures of the Fe_3O_4-SSZ NPs with Fe_3O_4 concentrations of 20, 50, 100, 200 and

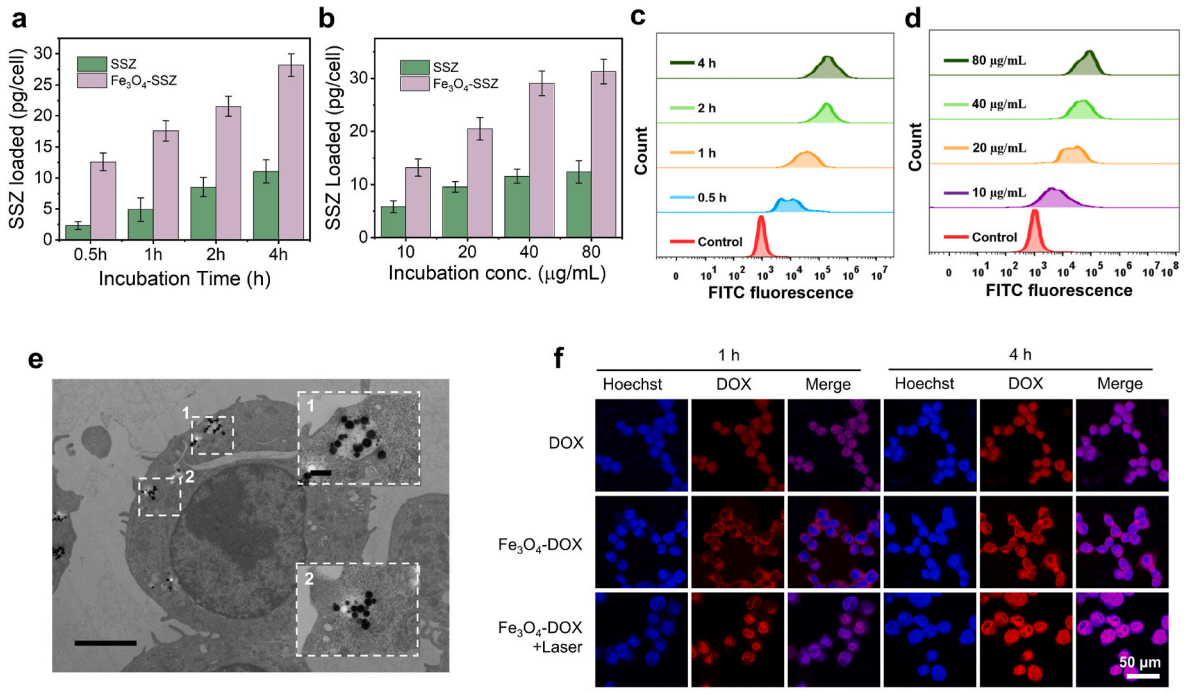

Fig. 2. (a) Contents of SSZ in the macrophages after incubation with SSZ and Fe_3O_4-SSZ NPs at SSZ concentration of 40 μg/mL for different times (0.5, 1, 2, and 4 h). (b) Contents of SSZ in the macrophages after incubation with SSZ and Fe_3O_4-SSZ NPs for 4 h at various SSZ concentrations of 10, 20, 40, and 80 μg/mL. (c) Flow cytometry analysis of macrophages after incubation with Fe_3O_4-FITC for different time (0.5, 1, 2, and 4 h). (d) Flow cytometry analysis of macrophages after incubation with Fe_3O_4-FITC at FITC concentrations of 10, 20, 40, and 80 μg/mL. (e) TEM images of macrophages after incubation with Fe_3O_4-SSZ NPs for 4 h. Scale bar, 2 μm. Inset scale bar, 100 nm. (f) CLSM images of macrophages after incubation with DOX and Fe_3O_4-DOX NPs for 1 and 4 h in the presence and absence of NIR laser irradiation.

500 μg/mL increased to 37.1, 41.8, 49.6, 58.5, and 63.6 °C, respectively. While the temperature of PBS was slightly increased to 28.3 °C (Fig. 1f). The temperature was also monitored by the infrared thermographic images (Fig. 1g). Then, the photostability of the Fe_3O_4-SSZ NPs was studied by repeated irradiation with indocyanine green (ICG) as control. ICG exhibited sharp decline in photothermal efficiency even after one cycle of laser irradiation (Fig. 1h). By contrast, photothermal effect of Fe_3O_4-SSZ NPs kept at relative stable level after five cycles of laser irradiation. Moreover, the NIR laser irradiation showed little influence on the magnetic response of the Fe_3O_4-SSZ NPs (Fig. S5). These results indicate the excellent photostability of the Fe_3O_4-SSZ NPs.

3.4. The release of SSZ from the Fe_3O_4-SSZ NPs

The release behavior of SSZ from Fe_3O_4-SSZ NPs was studied in different pH environments in the presence and absence of irradiation. The Fe_3O_4-SSZ NPs showed a pH sensitive release that the cumulative release rates in pH 5.3 and 7.4 in absence of NIR light were 51.4 % and 33.6 %, respectively (Fig. 1i). The accelerated release in pH 5.3 environment is probably due to the pH sensitive dissolution of Fe_3O_4 NPs. Since the Fe_3O_4 NPs dissolved and disintegrated to smaller particles after incubation in pH 5.3 solution for 24 h (Fig. S6). The Fe_3O_4-SSZ NPs also indicated thermo-sensitive release that the cumulative release rates in pH 5.3 and 7.4 increased to 70.2 % and 51.8 % after the 5 min irradiation. These results suggest that the release of SSZ can be triggered by the pH and NIR irradiation.

3.5. Loading of the Fe_3O_4-SSZ NPs in Mφ

The obtained Fe_3O_4-SSZ NPs were then endocytosed by macrophages to construct Fe_3O_4-SSZ loaded Mφ (Fe_3O_4-SSZ@Mφ). The loading capacities of Fe_3O_4 and SSZ were determined by measuring the intracellular iron and SSZ using ICP-OES and UV–Vis spectrophotometer, respectively. As shown in Fig. 2a, the macrophages showed time-dependent endocytosis. As the incubation time extended, the contents of iron and SSZ increased. After incubation for 4 h, the concentration of SSZ reached 28.2 pg/cell which was much higher than free SSZ. In addition, we evaluated the uptake at various concentrations (Fig. 2b). When incubated with Fe_3O_4-SSZ at SSZ concentrations of 10, 20, 40 and 80 μg/mL, the cellular SSZ contents at 4 h was 13.2, 20.5, 29.1 and 31.3 pg/cell, respectively. The tendency of uptake of SSZ was consistent with that of Fe contents, which was demonstrated in Fig. S7. It was worth noting that free SSZ showed lower drug internalization efficiency than nanoparticles, indicating the commendable ability of nanoparticles in improving the drug loading in live cells. When the Fe_3O_4-SSZ NPs concentration was over 40 μg/mL, no significant increase in loading capacity was found. Hence, 40 μg/mL was an optimized concentration for Fe_3O_4-SSZ loading. The phagocytosis was also monitored by flow cytometry using fluorescent FITC as indicator. As shown in Fig. 2c and d, similar time/concentration-dependent uptake behavior was observed. Based on the above results, the loading of Fe_3O_4-SSZ NPs in Mφ was carried out at the SSZ concentration of 40 μg/mL with incubation time for 4 h. The phagocytosis of the Fe_3O_4-SSZ NPs could be observed by the TEM images. As shown in Fig. 2e, Fe_3O_4-SSZ NPs were located in the cytoplasm after the incubation, while no NPs were found in the nucleus.

The phagocytosis result was further studied by CLSM. In the CLSM experiment, Fe_3O_4 NPs were labeled with DOX, a fluorescent drug with strong nuclear affinity. As shown in Fig. 2f, free DOX was primarily located in the nuclei after incubation for 1 h and 4 h, while the Fe_3O_4 NPs were distributed in the cytoplasm. This result indicates the negligible release of the DOX. After NIR light irradiation, strong DOX fluorescence was observed in the nuclei, implying the laser triggered release of the DOX. The internalization efficiency of the DOX loaded Fe_3O_4 NPs was quantitatively studied by flow cytometry. As shown in Fig. S8, Fe_3O_4-DOX NPs exhibited higher cell uptake than free DOX, indicating the superior phagocytosis capacity than free drug.

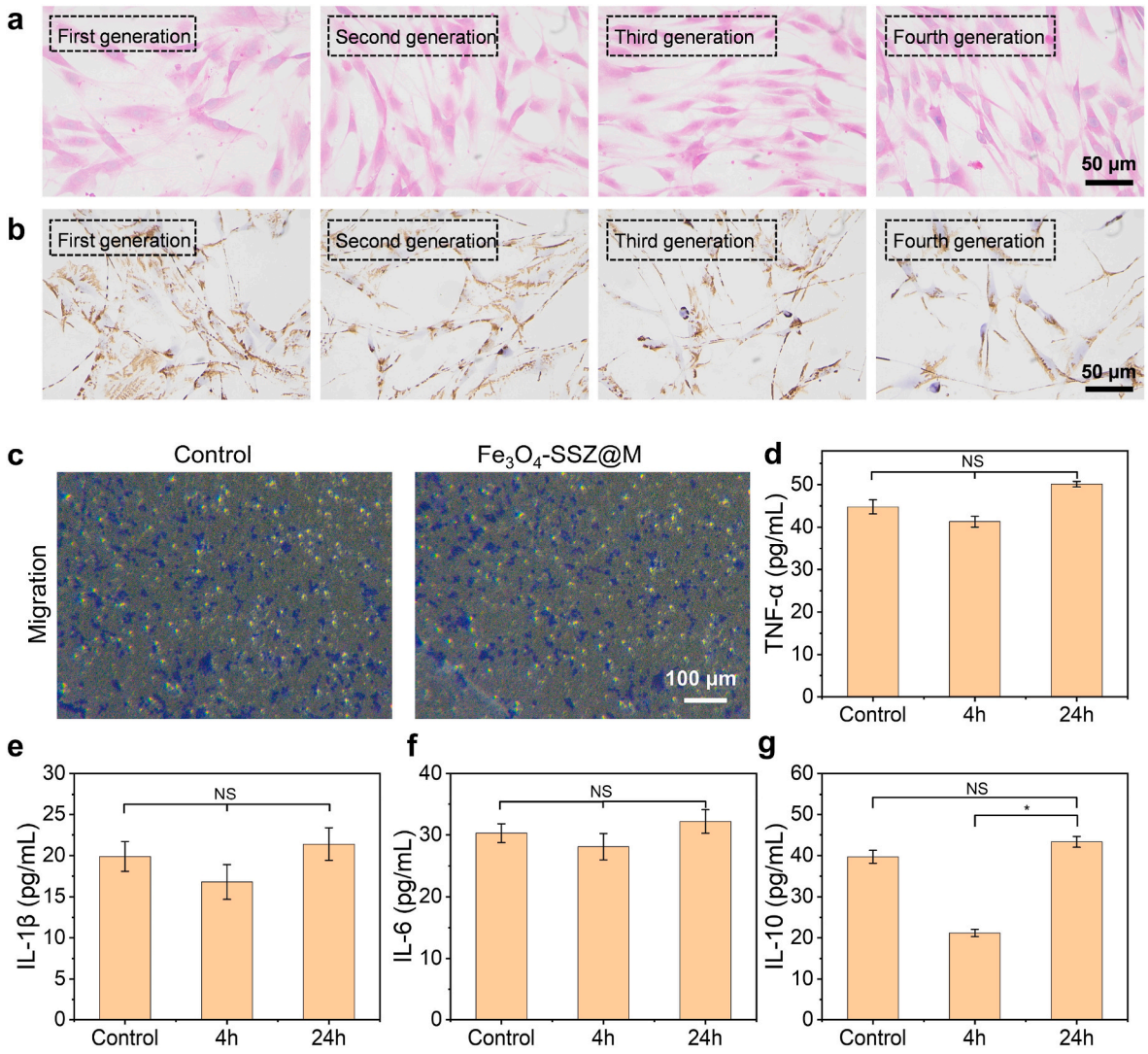

Fig. 3. (a) HE staining of FLSs isolated from CIA mice. (b) Representative immunostaining images of FLSs showing the vimentin. (c) Transmigration of untreated macrophages and macrophages loaded with Fe_3O_4-SSZ. Secretion of (d) TNF-α, (e) IL-1β, (f) IL-6, and (g) IL-10 from macrophages loaded with Fe_3O_4-SSZ at 4 h and 24 h. NS, not significant. $^*p < 0.05$.

3.6. Cell migration assay

The FLSs isolated from mice and the morphology (first to fourth generations) were imaged by microscope. As shown in Fig. S9, FLSs grew in colonies and were spindle shaped, parallel arranged. After HE staining, the oval nuclei were stained blue and located in the center of the cytoplasm (stained red) (Fig. 3a). The immunohistochemical experiment was also performed to study the presence of vimentin, a characteristic of fibroblasts from RA [28]. As shown in Fig. 3b, the cells were vimentin-positive, indicating the cells were FLSs. The above results suggest that the synovial fibroblasts were successfully isolated. Migration ability is critical for Mφ to deliver the drug into RA tissue and may be affected by the Fe_3O_4-SSZ NPs. The influence of Fe_3O_4-SSZ on the migration of Mφ was evaluated by a transwell experiment. The Mφ and Fe_3O_4-SSZ@Mφ were placed on the upper chamber of the device and the synoviocytes were seeded onto the lower chamber. As shown in Fig. 3c, Fe_3O_4-SSZ@Mφ could transmigrate the wells efficiently which was comparable to untreated Mφ cells, indicating ignorable effect of Fe_3O_4-SSZ NPs on the migration of Mφ.

3.7. Macrophage phenotype characterization

Macrophages commonly exist in two distinct subsets: M1 and M2 macrophages, characterized by the secretion of pro-inflammatory cytokines TNF-α, IL-6, IL-1β, and anti-inflammatory cytokines IL-10, respectively. We investigated the effect of Fe_3O_4-SSZ on macrophage phenotypes. The phenotypes of macrophage were determined by measuring the cytokines of TNF-α, IL-6, IL-1β, and IL-10. After incubation with Fe_3O_4-SSZ, no significant difference in the secretion of TNF-α, IL-6, IL-1β, and IL-10 was observed, suggesting the ignorable influence of Fe_3O_4-SSZ on the macrophage phenotype (Fig. 3d–g). Meanwhile, we detected the morphology of the macrophages after incubation. As shown in Fig. S10, the macrophages kept at a consistent morphology after the treatment of Fe_3O_4-SSZ. As a contrast, pro-inflammatory M1 phenotype was observed after the treatment of LPS, which was a classic agent to induce M1 polarization.

3.8. Cytotoxicity of Fe_3O_4-SSZ to Mφ

The cytotoxicity of free SSZ, Fe_3O_4 and Fe_3O_4-SSZ NPs to macrophages was evaluated in the presence and absence of NIR laser by MTT method. No obvious toxicity was observed for the SSZ and Fe_3O_4 group

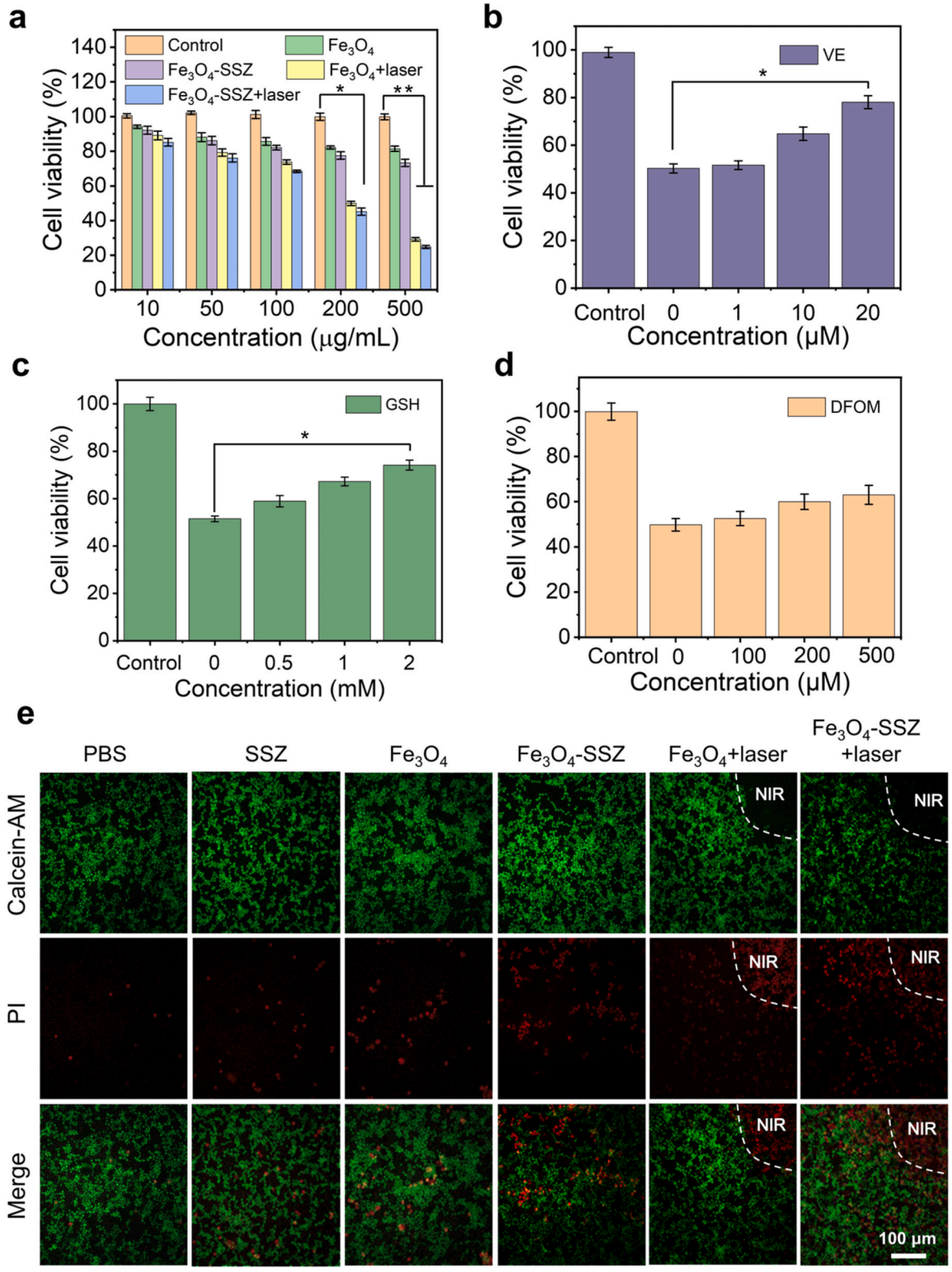

Fig. 4. (a) Cell viability of macrophages after incubation with Fe_3O_4, SSZ and Fe_3O_4-SSZ of different concentrations in the presence or absence of NIR irradiation. Cell viabilities of macrophages treated with Fe_3O_4-SSZ and H_2O_2 (100 μM) in the presence of (b) VE, (c) GSH, or (d) DFOM. (e) The images of macrophages stained with calcein-AM/PI showing the dead/live cells after incubation with PBS, SSZ, Fe_3O_4 and Fe_3O_4-SSZ in the presence or absence of NIR irradiation. *P*-values were calculated using two-sided unpaired *t*-test (*$P < 0.05$, **$P < 0.01$).

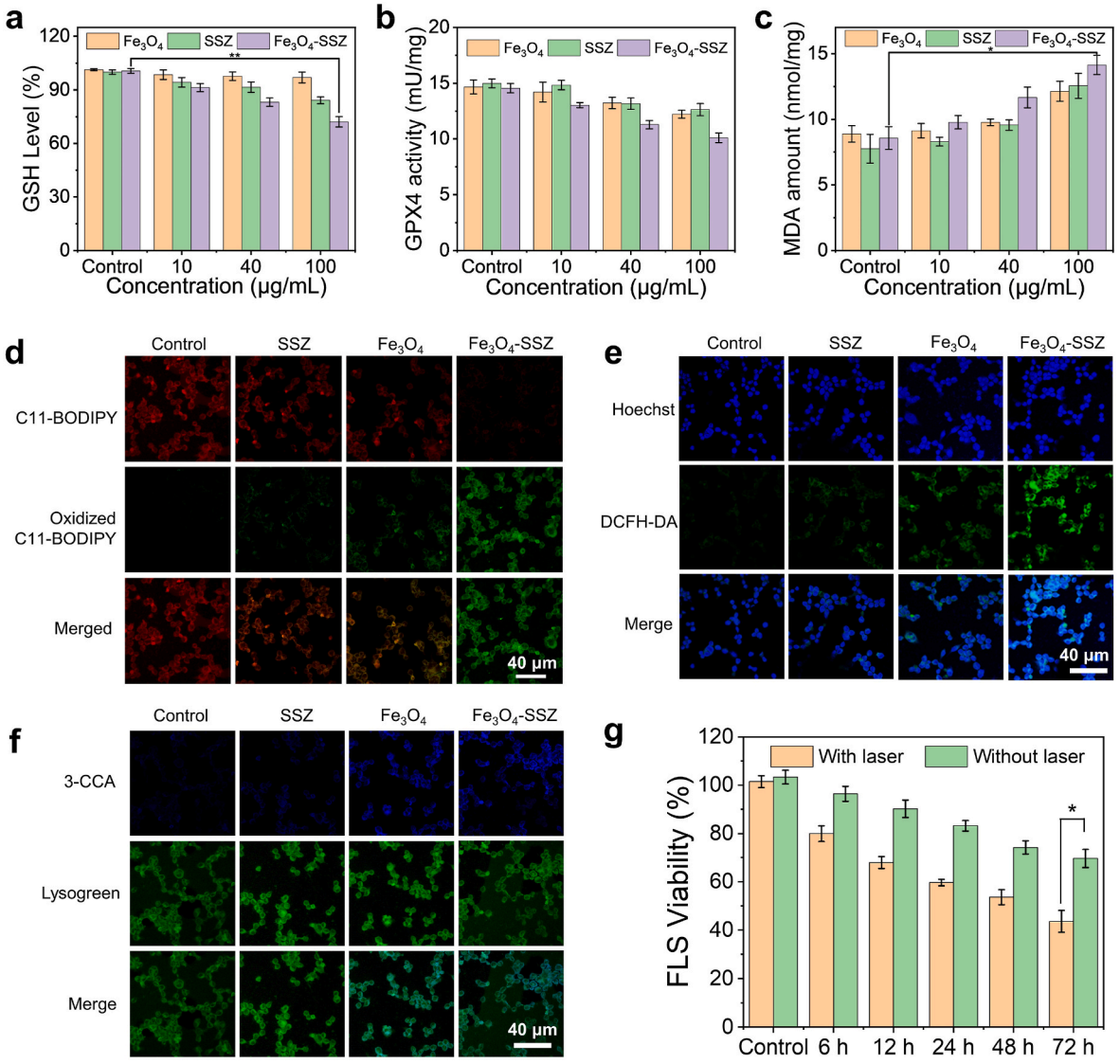

Fig. 5. The levels of (a) GSH, (b) GPX4 activity, and (c) MDA in macrophages after the incubation with Fe_3O_4, SSZ and Fe_3O_4-SSZ at different concentrations (10, 40 and 100 μg/mL). (d) CLSM images of macrophages stained with C11-BODIPY$^{581/591}$ showing the lipid peroxidation. The cells were incubated with SSZ, Fe_3O_4 and Fe_3O_4-SSZ NPs. CLSM images of macrophages stained with (e) DCFH-DA and (f) 3-CCA showing the intracellular ROS and •OH after treatments with SSZ, Fe_3O_4 and Fe_3O_4-SSZ. (g) Cytotoxicity of Fe_3O_4-SSZ@Mφ culture media at 6, 12, 24, 48 h, and 72 h towards FLSs in the presence and absence of NIR laser. *P*-values were calculated using two-sided unpaired *t*-test (*$P < 0.05$, **$P < 0.01$).

that the cell viability was over 85 % even at SSZ concentration of 70 μg/mL (Fig. S11a) and Fe_3O_4 concentration of 500 μg/mL (Fig. 4a). When the SSZ and Fe_3O_4 were co-delivered by Fe_3O_4-SSZ, the cytotoxicity was enhanced. Even though, the viability was over 75 %, which laid a foundation for Mφ to be loaded with Fe_3O_4-SSZ (Fig. 4a). The enhanced toxicity should be attributed to the synergistic effect of ferroptosis. SSZ is a competitive inhibitor of the xc^- transport system, which inhibits the transport of cysteine into cells, leading to the deficiency of antioxidant GSH and GPX4. While, Fe_3O_4 NPs release Fe^{2+} in acid condition, catalyzing the Fenton reaction to produce highly toxic •OH. When macrophages incubated with H_2O_2 (100 μM) and Fe_3O_4-SSZ, the cell viabilities further decreased to 51.3 % (Fig. S11b). The SSZ and Fe_3O_4 NPs generated combined lipid peroxidation and ferroptosis effect in the cells. We further studied the photothermal effect on the cytotoxicity. As shown in Fig. 4a, Fe_3O_4 + laser group exhibited superior toxicity showing cell viability of 35.2 % when the concentration reached 500 μg/mL. We also noticed that the cytotoxicity of Fe_3O_4-SSZ + laser was stronger than Fe_3O_4 + laser group, indicating the combined ferroptosis and photothermal effect (Fig. 4a).

The cytotoxicity of Fe_3O_4-SSZ could be remarkably inhibited by vitamin E (VE), a kind of liposoluble antioxidant. When the VE concentration elevated from 0 to 20 μM, the cell viability increased from 49.73 % to 78.09 % (Fig. 4b). This result indicates that the cytotoxicity should be attributed to the generation of ROS. It is reported that SSZ induces ferroptosis by inhibiting the synthesis of GSH. Hence, we evaluated the effect of supplemented GSH on the toxicity of Fe_3O_4-SSZ. As shown in Fig. 4c, GSH could obviously alleviate the toxicity of Fe_3O_4-SSZ. When the GSH concentration reached 2 mM, the cell viability increased by 22.7 %. This result indicates the mechanism of SSZ induced ferroptosis. What's more, we studied the effect of deferoxamine mesylate (DFOM, an iron chelation agent) on the toxicity of Fe_3O_4-SSZ. As shown in Fig. 4d, although the DFOM could inhibit the ferroptosis induced by Fe_3O_4-SSZ, the protective effect was limited when compared with VE and GSH. This is probably because DFOM can only chelate the iron ion to prevent the generation of •OH, while fails to scavenge other free radicals such as H_2O_2, $^1O_2$. These results were consistent with the Live/Dead cell staining (Fig. 4e). The macrophages treated with SSZ and Fe_3O_4 NPs were stained green suggesting the alive state. Moderate cell

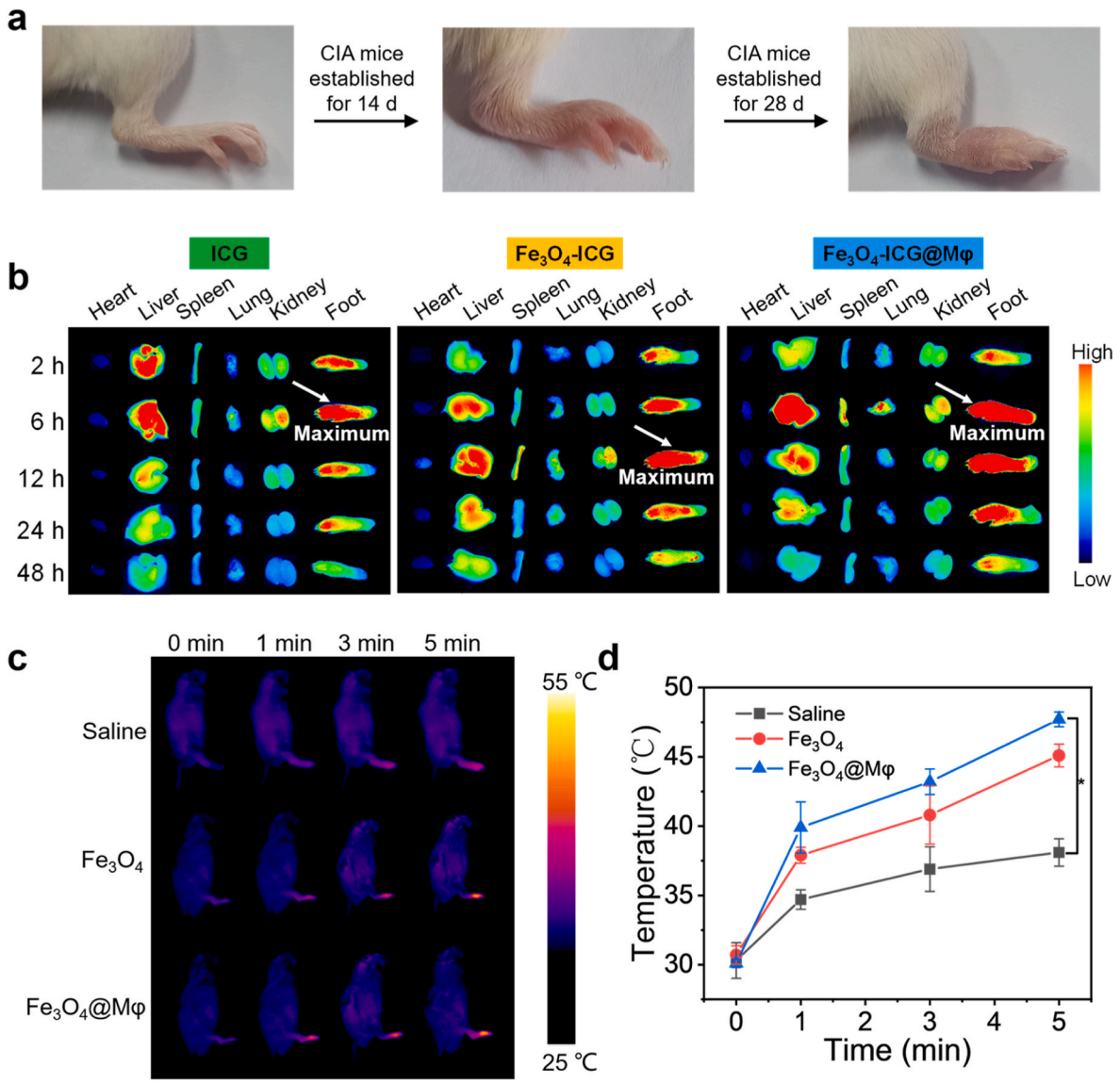

Fig. 6. (a) The digital images of arthritis modeling process at day 0, day 14 and day 28. (b) The fluorescence images of main organs and inflamed joints after intravenous injection of ICG, Fe_3O_4-ICG NPs and Fe_3O_4-ICG@Mφ. (c) *In vivo* thermographic images of CIA mice after irradiation with 808 nm laser at a power intensity of 2 W/cm^2 for 5 min. The PTT was carried out at 24 h post intravenous injection of saline, Fe_3O_4 and Fe_3O_4@Mφ. (d) Temperature curve of CIA mice during the PTT. *P*-values were calculated using two-sided unpaired *t*-test (*$P < 0.05$).

killing effect was observed in Fe_3O_4-SSZ NPs group as indicated by the emergence of red fluorescence. Fe_3O_4 + laser and Fe_3O_4-SSZ + laser leaded to serious damage due to the photothermal effect. We also noticed that cells in the region around the NIR laser spot in Fe_3O_4-SSZ + laser groups were also damaged, implying the combined PTT and ferroptosis therapy.

3.9. Intracellular GSH, GPX4 and MDA

To explore the toxic mechanism of the Fe_3O_4-SSZ, intracellular GSH, GPX4 and MDA were detected. As shown in Fig. 5a, Fe_3O_4 exhibited negligible effect on the level of intracellular GSH. By contrast, remarkably decrease of GSH was found in the SSZ and Fe_3O_4-SSZ group, showing the decreases by 15.7 % and 27.9 %, respectively. Pronounced decline of GSH in Fe_3O_4-SSZ group should be attributed to consumption of GSH by Fe^{2+} catalyzed ROS and the GSH synthesis inhibition induced by SSZ. In addition, the activity of GPX4 was further analyzed (Fig. 5b). The SSZ, Fe_3O_4 and Fe_3O_4-SSZ showed concentration dependent inactivation on the GPX4. Fe_3O_4-SSZ NPs displayed superior inhibitory effect due to the combined Fe^{2+} and SSZ effect. The depletion of GSH and the inactivation of GPX4 will induce lipid peroxidation and the generation of malondialdehyde (MDA). Hence, we further detected the intracellular MDA to study the lipid peroxidation (LPO). As shown in Fig. 5c, the amount of MDA in the Fe_3O_4-SSZ treated group elevated remarkably with the increase of concentrations. At the concentration of 100 μg/mL, the content of MDA increased by 1.6 times in comparison with the control group. Meanwhile, the content of MDA in Fe_3O_4-SSZ group was higher than those of Fe_3O_4 and SSZ groups, indicating the superior ability in inducing LPO. The LPO was also characterized by C11-BODIPY$^{581/591}$, an oxidation-sensitive and LPO-specific fluorescent probe generally accumulates in the cell membrane. Upon oxidization, the maximum emission peak of C11-BODIPY$^{581/591}$ will transfer from 590 nm (red) to 510 nm (green). CLSM images in Fig. 5d revealed the decay of the red fluorescence and the enhancement of green fluorescence in all the three groups. Strongest green fluorescence was observed in Fe_3O_4-SSZ group, demonstrating the synergistic effect of Fe_3O_4 and SSZ in inducing the LPO.

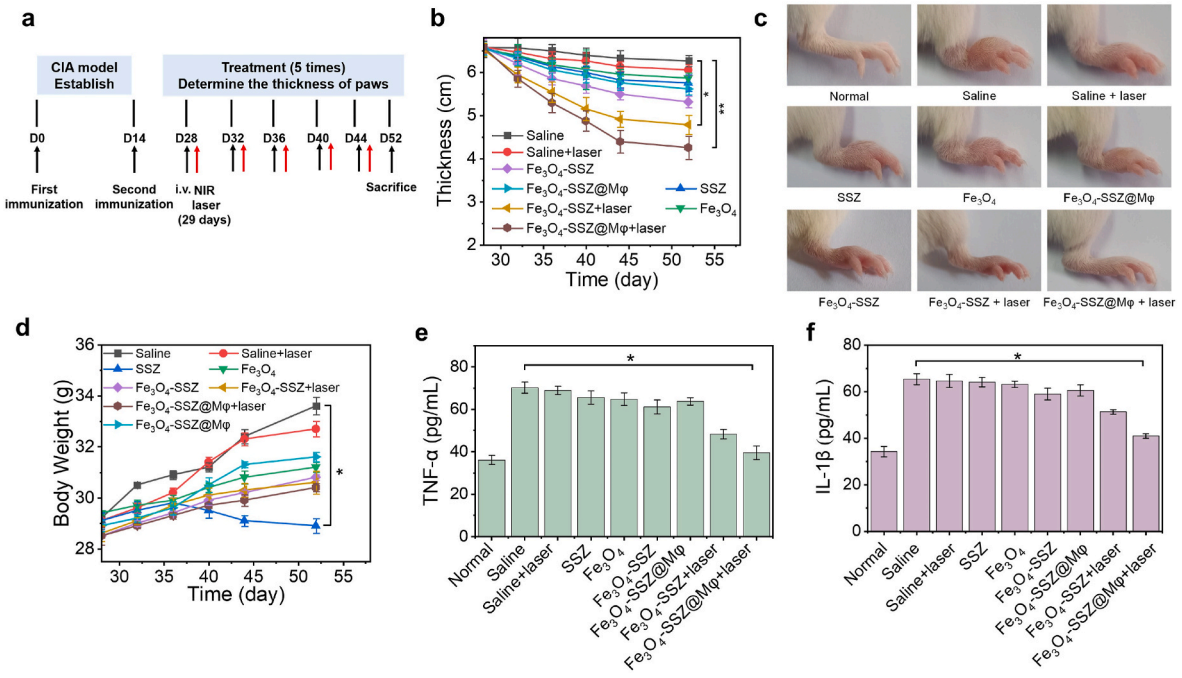

Fig. 7. (a) Schematic diagram showing the protocol of RA therapy. (b) Diameters of the paws during the different treatments. (c) Digital images of paws at the end of the treatments. (d) The body weight of the mice during the treatment. The (e) TNF-α and (f) IL-1β levels in serum after different treatments. P-values were calculated using two-sided unpaired *t*-test (**$P < 0.01$, ***$P < 0.01$).

3.10. Intracellular ROS detection

SSZ, Fe_3O_4 and Fe_3O_4-SSZ induced generation of ROS was investigated. The intracellular ROS was detected using DCFH-DA as probe, which is nonfluorescent and can be oxidized to fluorescent DCF. As shown in Fig. 5e and S12, green fluorescence could be observed in macrophages treated with SSZ, Fe_3O_4 and Fe_3O_4-SSZ. While, the fluorescence intensity of Fe_3O_4-SSZ group was stronger than SSZ and Fe_3O_4 group due to synergistic ferroptosis effect. The Fe^{2+} released from Fe_3O_4 NPs can catalyze the Fenton reaction to produce highly toxic •OH. We measured the intracellular •OH using 3-CCA as probe. Blue fluorescence with similar intensity was observed in Fe_3O_4-SSZ and Fe_3O_4 group (Fig. 5f). In sharp contrast, no noticeable fluorescence was detected in the control and SSZ group ((Fig. 5f and S13). These results indicate that Fe_3O_4-SSZ NPs are more efficient in inducing ROS and also explanation for the higher cytotoxicity.

3.11. Cytotoxicity of Fe_3O_4-SSZ@Mφ against FLSs

FLSs isolated from synovial tissue were utilized to evaluate the therapeutic effect of Fe_3O_4-SSZ@Mφ *in vitro*. The released drugs collected from Fe_3O_4-SSZ@Mφ triggering by NIR laser were incubated with the FLSs to study the cytotoxicity of Fe_3O_4-SSZ@Mφ. We observed time-dependent increase of cytotoxicity to FLSs. The medium collected from Fe_3O_4-SSZ@Mφ at 48 h presented a remarkable cytotoxicity to FLSs with viability decreased to 54.73 %, and cytotoxicity further decreased to 43.57 % at 72 h, while medium of 6 h showed little antiproliferative activity (Fig. 5g). These findings suggest that the Fe_3O_4-SSZ NPs, which were released from Mφ in response to the NIR laser stimuli, can effectively deliver into the FLSs to produce synthetic ferroptosis and photothermal effect.

3.12. In vivo biodistribution assay

The collagen induced arthritis (CIA) model mice were induced by immunization with type II collagen in complete Freund's adjuvant (CFA). After immunization, it takes 28 days for the arthritis to establish. The digital images of the paws were shown in Fig. 6a. The thicknesses of paws were measured by a vernier caliper at predetermined time points (0, 7, 14, 21, 28, 44 and 52 d) (Fig. S14). After immunization for 28 days, the thickness of CIA mice paws increased to 6.59 cm which was much higher than that of normal mice (2.64 cm). Over the next 24 days, the diameter of the paws was slightly decreased to 6.12 cm, indicating that RA could not self-recover.

The targeting effect of Fe_3O_4-ICG@Mφ was investigated in CIA mice using ICG as fluorescence probe. As shown in Fig. 6b, maximum distribution of free ICG and Fe_3O_4-ICG in joints were observed at 6 and 12 h post-injection, while Fe_3O_4-ICG@Mφ reached the highest distribution at 6 h post-injection. The fluorescence in Fe_3O_4-ICG@Mφ group was much stronger than free ICG and Fe_3O_4-ICG groups, suggesting targeting effect of macrophages towards RA. In addition, Fe_3O_4-ICG@Mφ demonstrated a retention over 48 h in the inflamed joints, which was much longer than the free ICG. The above results were consistent with quantitative analysis of mean fluorescence intensity (Fig. S15) indicating that macrophages can improve the arthritis targeting effect and extend the residence in the inflamed joints.

3.13. In vivo photothermal study

In vivo photothermal effect was performed to evaluate photothermal efficiency of NPs in CIA mice. Mice were intravenously injected with saline, Fe_3O_4, and Fe_3O_4@Mφ and irradiated with 808 nm laser at 24 h post injection. As shown in Fig. 6c, the temperatures of the joints were efficiently elevated in Fe_3O_4 and Fe_3O_4@Mφ groups after irradiation for 5 min, reaching 45.1 and 47.7 °C, respectively. In contrast, the temperature of the joint in saline slightly increased from 30.3 to 38.1 °C. The specific temperatures during the irradiation were shown in Fig. 6d. The higher temperature of Fe_3O_4@Mφ group should be attributed to the improved targeting effect and the enhanced accumulation in the RA tissue caused by the chemotaxis of macrophages.

3.14. Therapeutic effect of Fe_3O_4-SSZ@Mφ in CIA mice

The *in vivo* combined photothermal and ferroptosis therapy of Fe_3O_4-

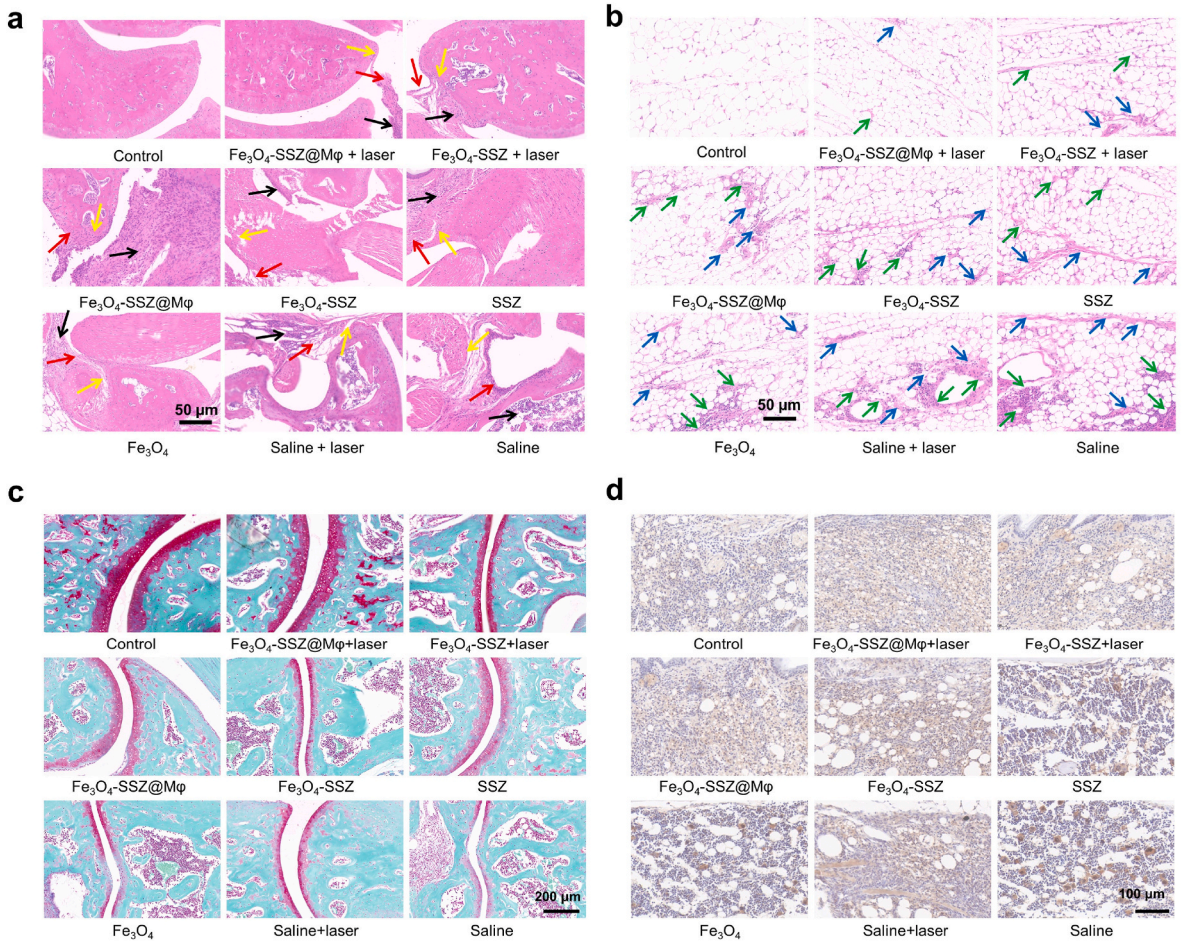

Fig. 8. H&E stained slice images showing the histopathology changes of (a) joint and (b) synovial tissue after different treatments. The black, red, yellow, green and blue arrows indicate infiltrated inflammatory cells, hyperplasic synovial, damaged cartilage, inflammatory cell and pathological vessel, respectively. (c) Representative Safranin O-fast green staining images. (d) Immunohistochemical staining for GPX-4 (brown) in the joint.

SSZ@Mφ was performed in CIA mice. The mice were randomly divided into eight groups: saline, saline + laser, SSZ, Fe_3O_4, Fe_3O_4-SSZ, Fe_3O_4-SSZ + laser, Fe_3O_4-SSZ@Mφ, Fe_3O_4-SSZ@Mφ + laser. The schedule for the treatment was shown in Fig. 7a. Fe_3O_4-SSZ exhibited obvious inhibition effect on the joint arthritis, with the paws thickness decreased from 6.59 cm to 5.31 cm. While the paws thicknesses in Fe_3O_4 and SSZ groups were 5.86 and 5.75 cm, respectively (Fig. 7b). Photothermal therapy could remarkably enhance the therapeutic effect. With the irradiation of NIR laser, the paws thicknesses of Fe_3O_4-SSZ and Fe_3O_4-SSZ@Mφ reduced from 5.31 cm to 5.61 cm–4.78 cm and 4.25 cm, respectively. We also noticed an interesting phenomenon that although Fe_3O_4-SSZ exhibited better effect than Fe_3O_4-SSZ@Mφ in absence of the NIR laser, Fe_3O_4-SSZ@Mφ showed more pronounced effect in the presence of NIR laser. This is probably because the encapsulation by Mφ slowed down the release of drug and weakened the ferroptosis effect. However, upon the irradiation of NIR laser, the Mφ was damaged and the drug in the RA tissue was burst released, resulting superior therapeutic effect. In the saline and laser groups, only slight decrease of the thickness was observed. The inflamed joints and mean arthritis score after the treatment were also vividly shown in Fig. 7c and Fig. S16, which were consistent with the results of paws thickness. During the therapy, the body weight of the mice was recorded to monitor the toxicity (Fig. 7d). SSZ exhibited strong toxicity to mice, however, the toxicity was relieved by loading onto Fe_3O_4 NPs due to the altered biodistribution and decreased release rate.

Pro-inflammatory cytokines contribute to RA pathogenesis and can be used as surrogate markers of therapeutic efficacy. We detected the pro-inflammatory cytokines (TNF-α and IL-1β) in the serum to further evaluate the therapeutic efficacy. As shown in Fig. 7e and f, lowest levels of TNF-α and IL-1β were observed in the Fe_3O_4-SSZ@Mφ + laser group. While, Fe_3O_4 + laser and Fe_3O_4-SSZ demonstrated limited effect in decreasing the pro-inflammatory cytokines. No perceptible effect was found in other groups. These results might be because the treatment of Fe_3O_4-SSZ@Mφ + laser could damage the hyperplastic FLSs and the infiltered inflammatory cells to alleviate the inflammation.

After the treatment, the joints were collected to perform the hematoxylin and eosin (HE) and S&O staining and immunohistochemical staining for GPX-4 analysis. As shown in Fig. 8a, histological staining of joints revealed massive synovial hyperplasia, extensive cartilage damage, and inflammatory cell infiltration in saline, saline + laser groups. Limited relief of the arthritis symptoms was found in SSZ, Fe_3O_4, Fe_3O_4-SSZ, and Fe_3O_4-SSZ@Mφ groups. By contrast, Fe_3O_4-SSZ@Mφ + laser markedly reduced the levels of synovial tissue hyperplasia and cartilage and bone destruction. From the HE images of the synovial tissue, we could clearly observe the infiltrated inflammatory cells and hyperplastic blood vessel in the saline, saline + laser groups (Fig. 8b). The inflammation in Fe_3O_4-SSZ@Mφ + laser groups was largely relieved, showing a synovial tissue that was comparable to the normal control group. Meanwhile, the Fe_3O_4-SSZ@Mφ exhibited excellent biocompatibility that no obvious toxicity to the major organs was found (Fig. S17). Safranin O-fast green staining results displayed the damage of cartilage (red) and subchondral bone (green) in Fe_3O_4-SSZ@Mφ + laser groups were minimal compared with saline group (Fig. 8c). The immunohistochemistry results demonstrated a decreased and uniformly distributed

of GPX-4 staining (brown) in the Fe_3O_4-SSZ@Mφ + laser group (Fig. 8d). These results confirmed that Fe_3O_4-SSZ@Mφ could achieve an excellent anti-RA efficacy by the synergistic ferroptosis and photothermal therapy without significant adverse effects on normal tissue.

4. Conclusion

In summary, a novel targeting delivery platform based on macrophages was developed to deliver Fe_3O_4 and SSZ for the ferroptosis and photothermal therapy of RA. Fe_3O_4-SSZ could be efficiently uptaken by the macrophages to increase the loading capacity of SSZ. Fe_3O_4-SSZ showed negligible toxicities towards Mφ and did not affect the migration and phenotype of Mφ. However, upon the irradiation of NIR laser, the Fe_3O_4-SSZ NPs killed the macrophages and FLSs efficiently by the combined effect of PTT and ferroptosis. Fe_3O_4 and SSZ NPs demonstrated pronounced ferroptosis effects by down-regulating GSH and GPX4 contents and increasing ROS and MDA level. In the biodistribution study, Fe_3O_4-SSZ@Mφ actively migrated to the inflamed site, showing an enhanced targeting and prolonged circulation effect. More importantly, Fe_3O_4-SSZ@Mφ inhibited the inflammation *in vivo* and demonstrated excellent therapeutic effects on RA. This live macrophage-based nanoplatform provides a strategy for the inflammation drug delivery, and also indicated the great potential of combined PTT and ferroptosis for RA therapy.

Credit author statement

Song Shen: Conceptualization, Funding acquisition, Methodology, Project administration, Supervision, Writing – review & editing. Xinxi Cai: Investigation, Methodology, Validation. Li Ruan: Investigation, Methodology, Writing – original draft. Jin Cao: Conceptualization, Supervision. Lin Wu: Conceptualization, Funding acquisition, Project administration, Writing – review & editing. Shifang Bei: Funding acquisition, Project administration. Rui Qian: Data curation, Investigation, Methodology.

Declaration of competing interest

The authors declare that they have no known competing financial interests or personal relationships that could have appeared to influence the work reported in this paper.

Data availability

Data will be made available on request.

Acknowledgments

This work was financially supported by the National Natural Science Foundation of China (Grants 82272662, 82003181 and 22074150), and Social Development Program of Zhenjiang City (SH2023051).

Appendix A. Supplementary data

Supplementary data to this article can be found online at https://doi.org/10.1016/j.mtbio.2023.100925.

References

[1] Q. Zhang, D. Dehaini, Y. Zhang, J. Zhou, X. Chen, L. Zhang, R.H. Fang, W. Gao, L. Zhang, Neutrophil membrane-coated nanoparticles inhibit synovial inflammation and alleviate joint damage in inflammatory arthritis, Nat. Nanotechnol. 13 (12) (2018) 1182–1190.
[2] M. Jeong, J.-H. Park, Nanomedicine for the treatment of rheumatoid arthritis, Mol. Pharm. 18 (2) (2021) 539–549.
[3] I.B. McInnes, G. Schett, Pathogenetic insights from the treatment of rheumatoid arthritis, Lancet 389 (10086) (2017) 2328–2337.
[4] J.S. Smolen, D. Aletaha, Rheumatoid arthritis therapy reappraisal: strategies, opportunities and challenges, Nat. Rev. Rheumatol. 11 (5) (2015) 276–289.
[5] S. Lin, Z. Zhou, C. Xu, F. Zeng, Z. Shi, J. Sun, X. Mei, C. Liu, D. Li, Cytokine regulation and fast inflammation resolution in early rheumatoid arthritis by cerium-modified gold nanoclusters, ACS Appl. Mater. Interfaces 14 (16) (2022) 18053–18063.
[6] P. Shah, A. Siddique, A. Thakkar, S. Gharat, A. Godad, P. Kale, G. Doshi, An update on novel therapeutic intervention in Rheumatoid arthritis, Int. Immunopharm. 109 (2022), 108794.
[7] A.B. Tu, J.S. Lewis, Biomaterial-based immunotherapeutic strategies for rheumatoid arthritis, Drug Deliv. Transl. Res. 11 (6) (2021) 2371–2393.
[8] Y. Li, Q. Liang, L. Zhou, J. Liu, Y. Liu, Metal nanoparticles: a platform integrating diagnosis and therapy for rheumatoid arthritis, J. Nanopart. Res. 24 (4) (2022) 84.
[9] Q. Zhang, D. Li, J. Zhong, Y. Wu, Y. Shi, H. Yang, L. Zhao, K. Yang, J. Lin, SPECT imaging and highly efficient therapy of rheumatoid arthritis based on hyperbranched semiconducting polymer nanoparticles, Biomater. Sci. 9 (5) (2021) 1845–1854.
[10] T. Nemeth, G. Nagy, T. Pap, Synovial fibroblasts as potential drug targets in rheumatoid arthritis, where do we stand and where shall we go? Ann. Rheum. Dis. 81 (8) (2022) 1055–1064.
[11] M. Conrad, D.A. Pratt, The chemical basis of ferroptosis, Nat. Chem. Biol. 15 (12) (2019) 1137–1147.
[12] H. Liang, X. Wu, G. Zhao, K. Feng, K. Ni, X. Sun, Renal clearable ultrasmall single-crystal Fe nanoparticles for highly selective and effective ferroptosis therapy and immunotherapy, J. Am. Chem. Soc. 143 (38) (2021) 15812–15823.
[13] W.S. Yang, B.R. Stockwell, Ferrootosis: death by lipid peroxidation, Trends Cell Biol. 26 (3) (2016) 165–176.
[14] C.A. Hitchon, H.S. El-Gabalawy, Oxidation in rheumatoid arthritis, Arthritis Res. Ther. 6 (6) (2004) 265–278.
[15] J. Li, F. Cao, H.-l. Yin, Z.-j. Huang, Z.-t. Lin, N. Mao, B. Sun, G. Wang, Ferroptosis: past, present and future, Cell Death Dis. 11 (2) (2020) 88.
[16] X. Chen, C. Yu, R. Kang, D. Tang, Iron metabolism in ferroptosis, Front. Cell Dev. Biol. 8 (2020), 590226.
[17] X. Zhu, Q. Chen, L. Xie, W. Chen, Y. Jiang, E. Song, Y. Song, Iron ion and sulfasalazine-loaded polydopamine nanoparticles for Fenton reaction and glutathione peroxidase 4 inactivation for enhanced cancer ferrotherapy, Acta Biomater. 145 (2022) 210–221.
[18] Y. Su, B. Zhao, L. Zhou, Z. Zhang, Y. Shen, H. Lv, L.H.H. AlQudsy, P. Shang, Ferroptosis, a novel pharmacological mechanism of anti-cancer drugs, Cancer Lett. 483 (2020) 127–136.
[19] H. Xin, Y. Huang, H. Tang, Y. Chen, H. Xia, F. Zhang, B. Li, Y. Ping, Delivery of a system x_c^- inhibitor by a redox-responsive levodopa prodrug nanoassembly for combination ferrotherapy, J. Mater. Chem. B 9 (35) (2021) 7172–7181.
[20] X. Chen, R. Kang, G. Kroemer, D. Tang, Broadening horizons: the role of ferroptosis in cancer, Nat. Rev. Clin. Oncol. 18 (5) (2021) 280–296.
[21] W. Wen, L. Wu, Y. Chen, X. Qi, J. Cao, X. Zhang, W. Ma, Y. Ge, S. Shen, Ultra-small Fe_3O_4 nanoparticles for nuclei targeting drug delivery and photothermal therapy, J. Drug Deliv. Sci. Technol. 58 (2020), 101782.
[22] S. Shen, F. Kong, X. Guo, L. Wu, H. Shen, M. Xie, X. Wang, Y. Jin, Y. Ge, CMCTS stabilized Fe_3O_4 particles with extremely low toxicity as highly efficient near-infrared photothermal agents for in vivo tumor ablation, Nanoscale 5 (17) (2013) 8056–8066.
[23] F. Xiong, Z.-y. Zhu, C. Xiong, X.-q. Hua, X.-h. Shan, Y. Zhang, N. Gu, Preparation, characterization of 2-Deoxy-D-glucose functionalized Dimercaptosuccinic acid-coated maghemite nanoparticles for targeting tumor cells, Pharm. Res. (N. Y.) 29 (4) (2012) 1087–1097.
[24] S. Shen, L. Wu, J. Liu, M. Xie, H. Shen, X. Qi, Y. Yan, Y. Ge, Y. Jin, Core-shell structured Fe_3O_4@TiO_2-doxorubicin nanoparticles for targeted chemo-sonodynamic therapy of cancer, Int. J. Pharm. 486 (1–2) (2015) 380–388.
[25] M. Xie, Y. Xu, H. Shen, S. Shen, Y. Ge, J. Xie, Negative-charge-functionalized mesoporous silica nanoparticles as drug vehicles targeting hepatocellular carcinoma, Int. J. Pharm. 474 (1–2) (2014) 223–231.
[26] M. Huo, Y. Zhao, A.B. Satterlee, Y. Wang, Y. Xu, L. Huang, Tumor-targeted delivery of sunitinib base enhances vaccine therapy for advanced melanoma by remodeling the tumor microenvironment, J. Controlled Release 245 (2017) 81–94.
[27] X. Zhang, L. Zhang, W. Xu, H. Qian, S. Ye, W. Zhu, H. Cao, Y. Yan, W. Li, M. Wang, W. Wang, R. Zhang, Experimental therapy for lung cancer: umbilical cord-Derived mesenchymal stem cell-mediated interleukin-24 delivery, Curr. Cancer Drug Targets 13 (1) (2013) 92–102.
[28] R. Vasko, J.H. Streich, S. Blaschke, G.A. Mueller, B. Mai, M. Kostrzewa, K. Sparbier, P. Korsten, S. Bohr, H. Dihazi, Vimentin fragments are potential markers of rheumatoid synovial fibroblasts, Clin. Exp. Rheumatol. 34 (3) (2016) 513–520.